KSCE Journal of Civil Engineering (2020) 24(8):2419-2434
DOI 10.1007/s12205-020-0107-1

pISSN 1226-7988, eISSN 1976-3808
www.springer.com/12205

Structural Engineering

Flexural Performance of Prestressed Beams with Grouting Material of Various Compactnesses

Xuansheng Cheng[a], Haibo Liu[b], Jiaxuan Su[c], Liang Ma[d], and Guoliang Li[a]

[a]*Western Engineering Research Center of Disaster Mitigation in Civil Engineering of Ministry of Education, Lanzhou University of Technology, Lanzhou 730050, China*
[b]*Key Laboratory of Disaster Prevention and Mitigation in Civil Engineering of Gansu Province, Lanzhou University of Technology, Lanzhou 730050, China*
[c]*Wenzhou Traffic Engineering Test and Inspection Limited Company, Wenzhou 310012, China*
[d]*Institute of Earthquake Protection and Disaster Mitigation, Lanzhou University of Technology, Lanzhou 730050, China*

ARTICLE HISTORY

Received 23 January 2019
Revised 8 January 2020
Accepted 15 April 2020
Published Online 30 June 2020

KEYWORDS

Prestressed beam
Sheath
Porosity
Ductility
Flexural performance

ABSTRACT

Presently, there is no reliable conclusion on the effect of grouting compactness on the mechanical behavior of a prestressed concrete structure. To study the influence of grouting compactness on the performance of prestressed concrete, the flexural behaviors of 8 prestressed beams fabricated by using different sheaths materials with grouting material of various compactnesses were studied experimentally, and the flexural bearing capacity and flexural stiffness of the prestressed beams were discussed. The results showed that the variation in the average strain along the beam height has a linear distribution. The load-deflection curves included two turning points, which indicate concrete cracking and steel yielding. The effect of grouting compactnesses on the early stage of beam cracking is small, but the effect becomes increasingly obvious after beam cracking. The distribution of cracks in the prestressed beams with fuller grouting is more concentrated compared to that of beams with lower grouting compactness; when the crack spacing is smaller, the beam ductility is reduced, and the bearing capacity is improved. The fracture resistance and overall bearing capacity of metal sheaths prestressed concrete beams are better than those of plastic sheaths prestressed concrete beams. However, the ductility of prestressed beams with plastic sheaths is better than that of prestressed beams with metal sheaths. A reference is provided for such prestressed concrete beams, but in practical engineering, the relevant parameters should be reevaluated because the number of studied samples is limited.

1. Introduction

Post-tensioned prestressed concrete structures have the advantages of high component rigidity, low material requirements, high crack resistance and durability, low self-weight, high crossing ability and easy assembly (Zhu, 2012). Post tensioning is gaining more acceptance in a variety of applications (e.g., cantilever construction, long-span construction or span-by-span construction), and post tensioned prestressed structures being implemented. Also, post tensioning concrete has been widely used in various modern buildings and bridge construction businesses. These post-tensioned prestressed concrete structures are widely used in certain long-span structures, such as bridges and beam cranes. Two examples include the Shanghai Xinghewan Middle School Comprehensive Building, and Guangdong Xiaolinghe Extra Large Bridge. The design and construction of long-span prestressed bridges have become a focus of contemporary social development (Du, 1997; Zhang, 2007). Statistically, there are more than half a million bridges in China; of these bridges, there are more than three hundred thousand highway bridges and nearly two hundred thousand railway bridges. During the construction of prestressed concrete structures, quality problems arise for various reasons, such as cracking during construction, damage of the structure before the expected lifespan is reached, and insufficient grouting of post-tensioning ducts that leads to steel strand corrosion. These issues directly affect the quality and durability of the

CORRESPONDENCE Xuansheng Cheng chengxslut@sina.com Western Engineering Research Center of Disaster Mitigation in Civil Engineering of Ministry of Education, Lanzhou University of Technology, Lanzhou 730050, China

© 2020 Korean Society of Civil Engineers

whole structure and can even cause accidents (Ji and Fu, 2010). In 1985, during the operation of the Ynys-y-Gwas Bridge in South Wales, England, the use of a post-tensioned prestressed concrete structure was suspended due to a sudden collapse in the bridge because of the uncompacted grouting at the site of the channel and the severe corrosion of the prestressed steel wire bundles. It has been recently observed that bridge collapse may be due to the porosity of the grouting material. This issue has drawn great attention across the bridge industry, and the post-tensioned prestressed concrete grouting problem has been listed as one of the top ten common issues in bridge construction (Woodward, 1990; Farhidzadeh and Salamone, 2015). An investigation into the grouting compactness of more than 8,000 channels showed that only 39 cases revealed completely dense grouting, while 13% were completely empty (no grouting), and 39% sustained serious corrosion of the steel strand due to the noncompaction of the grouting material (Wu and Liu, 2013). The quality of grouting in prestressed construction materials directly affects the durability, reliability and safety of prestressed structures.

Park et al. (2016) conducted experiments on five giant post-tensioned prestressed beams to study the effect of high-strength steel strands on the bending behavior of prestressed beams. The results showed that the bending behavior of the post-tensioned prestressed beams was in good agreement with the prediction results of the current codes regardless of the tensile strength of the strands. In order to investigate the flexural performance of post-tensioned prestressed ultra-high-strength concrete beams, Meng et al. (2013) carried out a test of the mechanical properties of post-tensioned prestressed ultra-high-strength concrete simply supported beams under vertical static loading. The research results can provide some theoretical basis for the design of post-tensioned ultra-high-strength concrete beams and the revision of relevant codes. Rupf et al. (2013) studied the mechanical behaviors of post-tensioned beams with 12 low-shear steel bars and flanges and described the experimental results of beam shear failure to analyze the important parameters that affect the shear strength and failure mode. Their experimental results were compared with the analysis results based on the elastoplastic stress field. Zhou et al. (2013) studied the influence of various factors on the seismic performance of the beam through low-cycle repeated loading tests of post-tensioned bonded prestressed concrete beams and then evaluated the rationality of relevant provisions on the seismic design of post-tensioned prestressed concrete structures. Enrin et al. (2000) conducted a static load and high-speed dynamic flexural toughness test to evaluate and compare the elastic-plastic performance and flexural toughness of pretensioned prestressed concrete beams and post-tensioned prestressed concrete beams. And the result showed that under the static loading condition and the same flexural strength of beams, the ultimate deformation of the post-tension prestressed reinforced concrete beam was clearly larger than the other two kinds of beams. Cao et al. (2013) used prestressed concrete beam components to study the whole bending process of prestressed concrete beams subjected to freezing-thawing damage by rapid freezing and thawing tests and analyzed the effect of the number of freeze-thaw cycles on the prestressed concrete beams by evaluating their bending performance. Deng and Shao (2013) proposed a hybrid element model of a nonlinear analysis of prestressed reinforced concrete beams by the corotating coordinate method and verified the correctness by using examples to show that, compared with traditional models, the proposed hybrid element model can better analyze the nonlinear performance of prestressed reinforced concrete beams. Dong (2010) carried out a theoretical and modeling test research on the deflection calculation of prestressed concrete beams after cracking, and gave the calculation method of deflection about cracked prestressed concrete simply supported beams based on the stepped stiffness characteristics. Based on the bending crack width test of 8 post-tensioned prestressed concrete beams, Du and Su (2012) performed a statistical analysis of crack widths at different locations based on the test results, obtaining the short-term crack width expansion coefficients and providing conversion calculation formula of crack width at different positions about post-tensioned prestressed concrete beams. Minh et al. (2007; 2008) did a series of experiments to show that chloride-induced corrosion of the sheaths and the post-tensioned prestressing tendon significantly decreases the load-carrying capacity of PC beams while proper grouting can protect a prestressing tendon from corrosion despite the wider cracks. Wang et al. (2014) studied the effect of insufficient grouting and steel strand corrosion on the flexural properties of prestressed concrete beams, showing that insufficient grouting (including voids, lengths and locations of areas without grout) affected the flexural properties of prestressed concrete. By doing some experiment (Feng et al., 2014; Zhou et al., 2014), they found that the ultrasonic method can effectively evaluate the grouting quality of prestressed bellows pore, which can provide a basis for the testing of grouting quality about prestressed bellows pore.

The existing studies on prestressed concrete technology in construction engineering focus on researching new materials, new equipment and new technologies to ensure the reliability of prestressed concrete construction, and it is believed that only grouting compactness has an impact on the structure. However, there is little research on the aspects of grouting compactness. In this paper, the application of prestressed grouting and its testing technology was reviewed to improve structural safety, and the bending resistance of these structures was mainly studied. The theoretical basis of post-tensioned prestressed concrete design and construction was provided by investigating the section strain, deflection, failure process and failure mode under different grouting compactnesses, and the change in the flexural bearing capacity and flexural rigidity under different grouting compactnesses was discussed. Although the results were obtained based on 8 beams, 4 of which include metal sheaths and 4 of which include plastic sheaths, there are some limitations in this study because the number of samples was limited. In addition, there are various uncertainties in the test process.

2. Test Setup

2.1 Specimen Design and Fabrication

This experiment used prestressed concrete beams made with the post-tensioned method. A total of eight prestressed concrete test beams were manufactured with the same size but with different sheaths materials and different degrees of grouting compactness. The specimen numbers and parameters were shown in Table 1. The section size was 150 mm × 250 mm, and the net span is 1,800 mm. The beams were made by pouring 35 MPa concrete into a prefabricated wood formwork using a vibrating rod to compact the material. Beams were left to cure until time of testing, 28 days. The longitudinal tension of the main reinforcement was created by using Φ10 of HPB300. According to the structural requirements, the upper part of the beam was equipped with 2Φ10 of 300 MPa. The stirrups used 300 MPa with Φ6@100, and the prestressed tendon used a Φ6(1 × 7-6)1270 steel strand. The distance between the prestressed tendon and the bottom edge of the beam was 50 mm, and the thickness of the concrete cover was 20 mm. Fig. 1 showed a diagram of the specimen size and reinforcement.

2.2 Material Properties

The parameters of the various materials and their related components used in this paper were as follows:

1. The prestressed steel strand was a 1 × 7-6-1270 galvanized steel strand; the nominal diameter is 6 mm, the nominal area was 22 mm^2, the tension control stress was 889 MPa, f_{pk} = 1270 MPa, and E_p = 2.05E + 5 MPa.
2. Cement: 42.5 grade ordinary Portland cement was used. See in Table 2 for the cement properties.
3. Sand: Medium-grained sand was used, and the content of mud was less than or equal to 3%.
4. Stone: Here, 5 – 20 continuously graded broken stones are used, and the content of mud was less than or equal to 1%.

2.3 Concrete Mixture

In this research, C35 concrete was used to design the concrete mix ratio according to 'Specification for mix proportion design of ordinary concrete' (JGJ55-2011, 2010), and the mix ratio was shown in Table 3.

2.4 Loading Device and Sensor Locations

The experimental loading adopted the portal-type vertical

Table 1. Specimen Numbers and Parameters

Number	Sheath material	Test beam number	Width (mm)	Height (mm)	Grouting compactness	Loading forms
1	Metal sheaths	PCB1-1	150	250	No grouting	Symmetrical load
2		PCB1-2	150	250	1/3	Symmetrical load
3		PCB1-3	150	250	2/3	Symmetrical load
4		PCB1-4	150	250	Fully compact	Symmetrical load
5	Plastic sheaths	PCB2-1	150	250	No grouting	Symmetrical load
6		PCB2-2	150	250	1/3	Symmetrical load
7		PCB2-3	150	250	2/3	Symmetrical load
8		PCB2-4	150	250	Fully compact	Symmetrical load

Note: For the prestressed concrete beams with 1/3 full grouting (PCB1-2, PCB2-2) and 2/3 full grouting (PCB1-3, PCB2-3), 1/3 and 2/3 of the cross-sections, respectively, were filled by the self-weight of the grouting body to achieve the effect in which the grouting is not full.

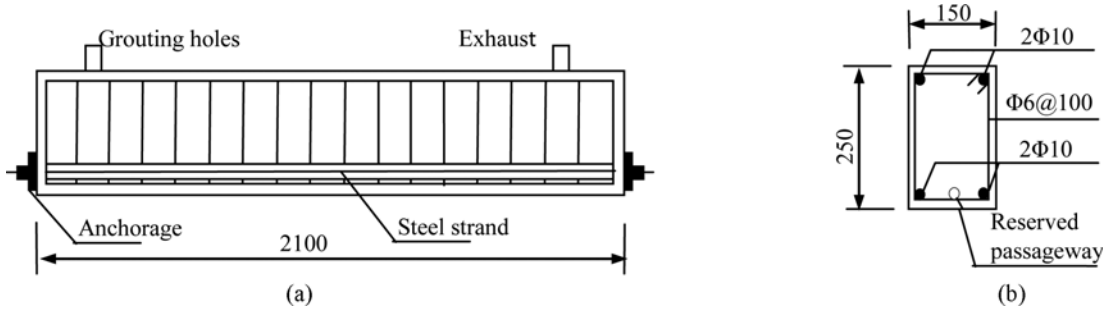

Fig. 1. Dimensions and Reinforcement Diagram of the Test Beams (mm): (a) Side View of Test Beam, (b) Normal Section of Test Beam

Table 2. Cement Properties

Cement fineness (m^2/kg)	Setting time (min)		Compression strength (MPa)		Rupture strength (MPa)	
	Initial setting	Final setting	3 d	28 d	3 d	28 d
350	173	238	27.3	51.6	6.0	7.4

Table 3. Concrete Mixture

Water to cement ratio W/C	Sand to coarse aggregate ratio (%)	Water (N/m^3)	Cement (N/m^3)	Sand (N/m^3)	Cobblestone (N/m^3)
0.41	39	1,646.4	4,008.2	6,987.4	10,927

loading device, using a predetermined loading rate. Before the prestressed beams were loaded, the beams were preloaded to check whether the instruments and collecting systems were functioning. The total load was 50 kN, and the load of each level was 10% of the total load. To accurately obtain the actual cracking load of the structure, the load of each stage was 5% of the total load until the load reaches 90% of the calculated cracking load (That is to say, from the beginning of loading to 90% of the calculated cracking load, data was recorded once for every 10% of the total load; when 90% of the calculated cracking load was reached, data is recorded for every 5% of the total load until the structure cracked.). After cracking, the specimen recovered, and loading continued at 10% of the total load, data is recorded once when every 10% of the total load was loaded; however, the specimen was loaded with 5% of the total load after reaching 90% of the total load, data is recorded every 5% of the total load until the structure broke. To accurately obtain the damage load of the member, the load was measured by the load cell until the specimen cannot continue to bear the load (Wang, 2013). After each stage of loading, the load was maintained for 10 min, the experimental phenomena were recorded, the crack width was measured, and the crack development was observed.

Figure 2 is a diagram of the sensor locations. Three concrete strain gauges were arranged on the side of the beam near the top, mid-height, and bottom at 1/2, 1/4, and 1/8 the beam span, for a total of 9 strain gauges, as shown in Fig. 2(a). At the same time, the concrete strain about the bottom of test beam was measured by using three concrete strain gauges at the 1/2, 1/4, and 1/8 of the bottom beam centerline, as shown in Fig. 2(b). The deflection of the test beam was measured by a WY-50 displacement sensor, which had a measuring range of 50 mm and a sensitivity of 200 με/mm. The displacement meter was installed on the beam span of the test beam at the 1/2 beam span, 1/4 beam span and 1/8 beam span, and the change in the deflection of the test beams under the load was measured. The vertical load applied by the hydraulic pump and jack loading system on the distribution beam can be directly measured by the load cells installed under the jack. The strain, displacement and load data were collected through the DH3816 acquisition system.

3. Test Results and Analysis

In this part, we studied the bending properties of post-tensioned prestressed concrete beams based on the experimental results, mainly analysis their failure process and failure pattern, changing law of strain, deflection, ductility, and stiffness.

3.1 Failure Process and Failure Pattern

During early stages of the test, prior to cracking, the beams exhibited a monotonic change in deflection with increased loading. When the load increased to the cracking load, for each test beam, the first vertical crack appeared in the middle part of the lower edge; then, the cracked prestressed beam begun to carry the load. As the load continued to increase, the crack width in the pure bending section of the member increased and gradually extended upward. New cracks appeared and moved successively outward from mid-span of the beam to the two supports of the beam, resulting in reduced beam capacity. The neutralization axis continued to move up the beam, and vertical cracks appeared directly below the loading points. Oblique cracks appeared between the loading points and the supports, and these cracks continued to appear and extended to the loading points as the load continues to increase. With the continuous increase in the load, the increase in deflection and crack width clearly accelerated, and the increase in the strain of the steel bar accelerated after yielding. This results in damage to the bond between the surfaces of the cracks in the concrete, and the cracks widened and extended upward. As loading continued, the stress of the steel

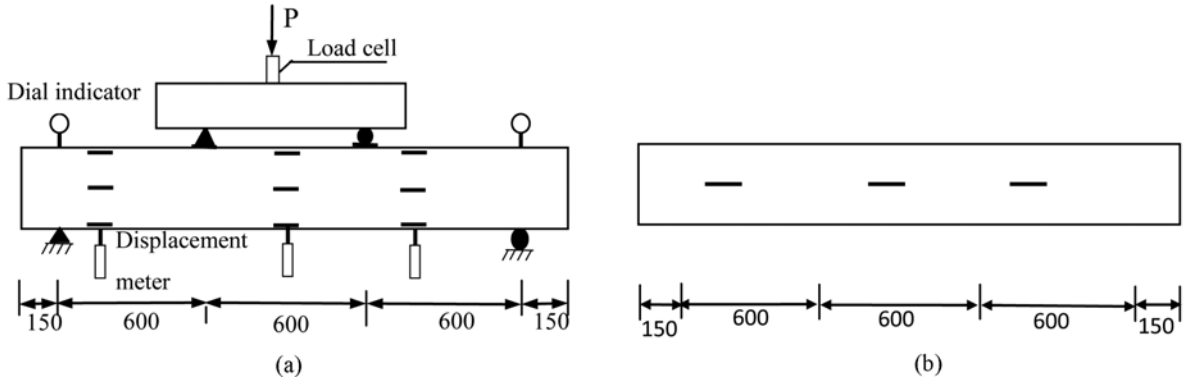

Fig. 2. Sensor Locations (mm): (a) Test Beam Side, (b) Bottom of the Test Beam

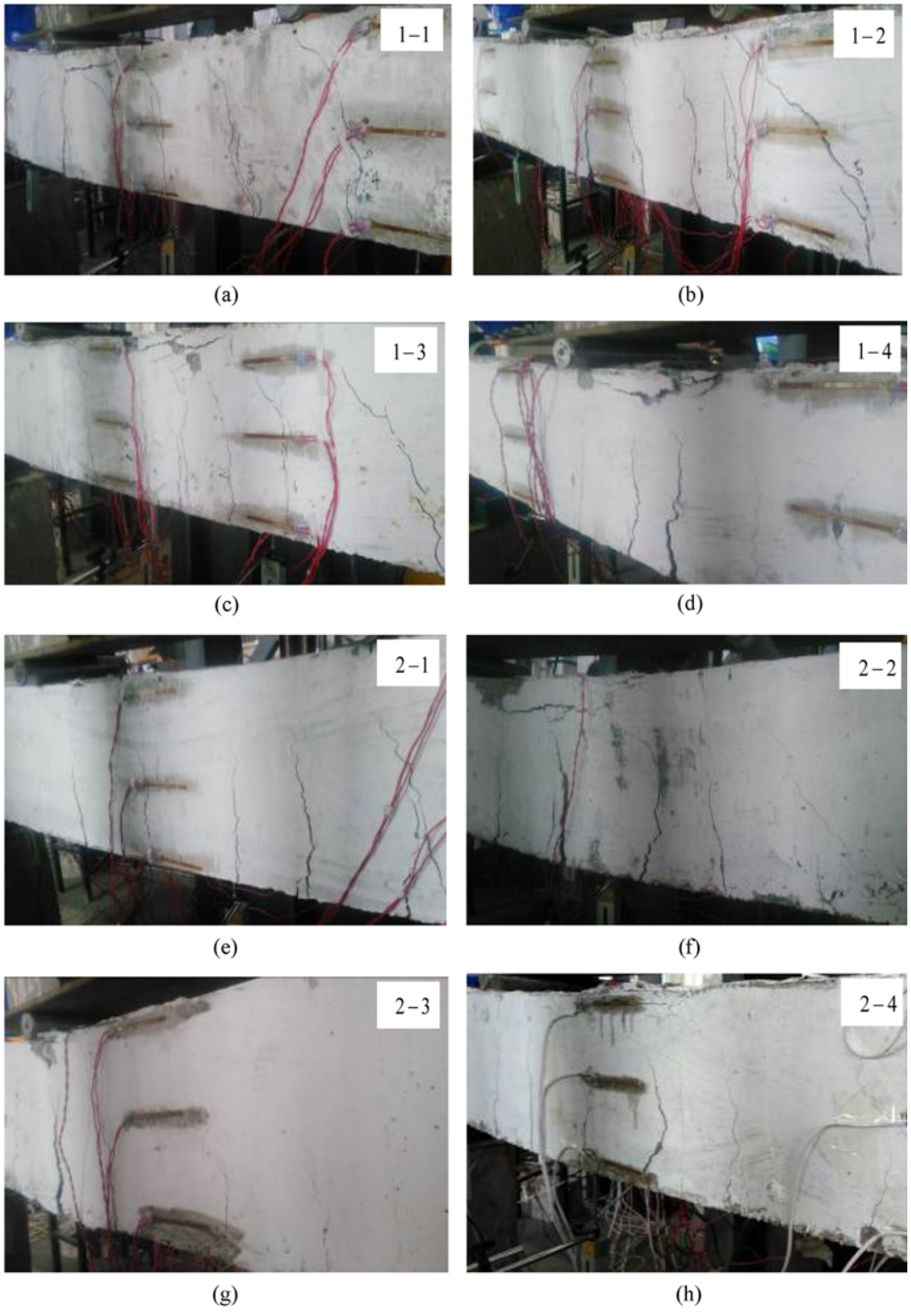

Fig. 3. Failure Patterns of the Specimens: (a) PCB1-1, (b) PCB1-2, (c) PCB1-3, (d) PCB1-4, (e) PCB2-1, (f) PCB2-2, (g) PCB2-3, (h) PCB2-4

bar remained unchanged, while the strain increased; the strain of the concrete in the compression zone increased until the concrete at the loading point of the upper part of the pure bending section of the prestressed beam member was crushed, and the bearing capacity sharply decreased. After the loading stopped, the development condition of cracks after the failure of each beam is shown in Fig. 3 (Failure refers to the state where the concrete at the upper loading point of the pure bend section about the prestressed beam is crushed suddenly when the load continues to increase to a certain stage and the bearing capacity is sharply reduced, this state can be observed clearly at this moment).

The phenomenon observed for each test beam was similar, and PCB1-3 was taken as an example. Under the action of a large load, when the load increased to 42.5 kN, vertical cracks first appeared in the middle part of the span of the lower edge of the test beam, and the midspan deflection reached 4.15 mm. As

Fig. 4. Diagonal Crack Development

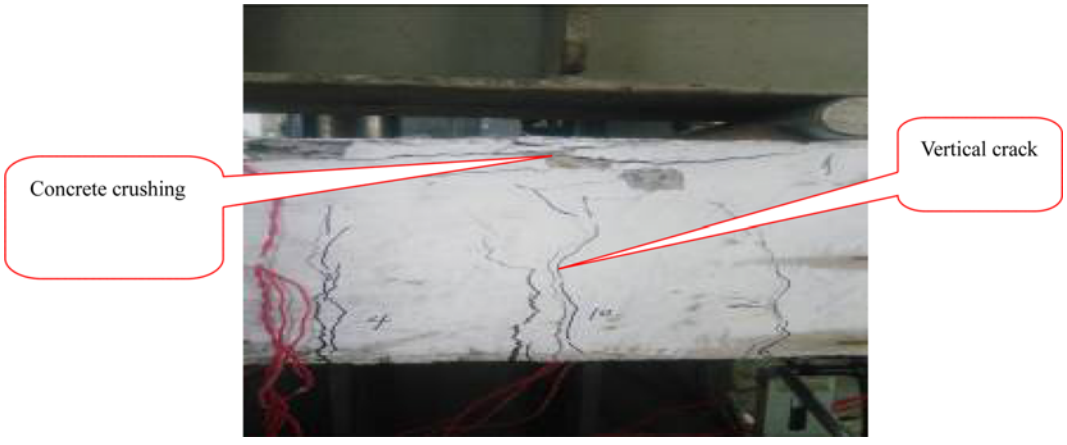

Fig. 5. Vertical Crack Development

Table 4. Test Results of the Beams under Different Loads

Number	Cracking load P_{cr} (kN)	Ultimate load P_u (kN)	Crack deflection (mm)	Maximum deflection (mm)	Fracture work (N • m)	Yield work (N • m)	Ductility coefficient
PCB1-1	31.6	79.1	3.61	20.38	1193.10	316.9	3.76
PCB1-2	36.8	86.8	3.92	22.03	1413.22	415.55	3.40
PCB1-3	42.5	93.2	4.15	24.46	1731.25	536.75	3.22
PCB1-4	45.3	103.7	4.35	27.20	2063.6	661.65	3.12
PCB2-1	28.7	77.3	3.41	18.01	900.02	204.87	4.39
PCB2-2	31.3	81.8	3.52	19.82	1091.85	280.05	3.90
PCB2-3	35.5	87.2	3.84	21.21	1262.12	357.42	3.53
PCB2-4	43.1	96.3	4.06	24.96	1717.67	518.4	3.31

the load continued to increase, the cracks gradually extended upward along the cracking direction. In addition, as new cracks appeared successively, the crack spacing decreased, and the vertical cracks appeared just below the loading point, as shown in Fig. 4. When the load increased to 93.2 kN, the concrete near the upper loading point of the pure bending section of the prestressed beam was crushed, and the bearing capacity of the concrete rapidly decreased. At this time, the deflection in the middle of the span reached 24.46 mm, as shown in Fig. 5. Table 4 showed the cracking load, crack deflection, ultimate load and maximum deflection of each test beam.

The work done during the fracture and yield of the concrete structure is calculated from the load-deflection curve (see in Fig. 14), and their work can be seen in Table 4. The greater the work done, the stronger the structure. Ductility is the deformation of a structure stepping into yield under external load and after the structure enters the plastic stage, the deformation continues to increase under the continued load but the structure won't be damaged. Therefore, the ratio of fracture work to yield work is used to measure the ductility of the structure. From Table 4, it can

be known that with the same sheaths material, as the grouting compactness increases, the energy consumption capacity of the prestressed concrete beam significantly increases, but the ductility coefficient gradually decreases. However, because the fuller grouting compactness of the structure, the stronger the bonding between the structures, the lower the possibility of weak surfaces, increasing the stiffness of the structure and reducing the ductility. The increased adhesion between the structures provides a larger tensile force for the concrete to achieve crack strength, reduces the crack spacing and increases the energy consumption of the structure. This view has been confirmed by some scholars (Jaime et al., 2018; Moini et al., 2018). Under the same grouting compactness, the energy consumption of prestressed concrete beam with metal sheaths is greater than that of prestressed concrete beam with plastic sheaths, and the ductility is smaller.

Through the experimental observation and analysis, under the action of a load, the failure of each test beam was caused by the crushing of the concrete in the compression zone after the tensile steel bars yield. Under the same grouting compactness, the bearing capacity of the prestressed beams with metal sheaths was higher than that of the prestressed beams with plastic sheaths, and the crack distribution in the beams with metal sheaths was more concentrated than that in the beams with plastic sheaths; in addition, the cracks were closely spaced. Using the same sheaths material, the bearing capacity of the prestressed concrete beams increased with the filling compactness. Additionally, the distribution of cracks became more concentrated, and the distance between the cracks decreased as the filling degree of the grouting increased. Possibly because in the fully grouted prestressed concrete beams, a strong bond existed between the prestressed tendons and the surrounding concrete, allowing the prestressed tendons in the midspan to more fully exert their tensile effect. Therefore, the bearing capacity of the prestressed specimen with a denser grouting material was greater because the prestressed tendons and the surrounding concrete maintain a bond stress, causing the prestressed tendons of the cracked section significantly increasing the strain. Therefore, the cracks were more concentrated, and the beam suffered from local damage earlier. However, the stress of the prestressed concrete beams with insufficient grouting was uniformly distributed along all of the prestressed tendons, possibly adjusting the strain within all of the prestressed tendons. The strain was nearly uniform, and the plastic hinge zone can bear the load more stably. Therefore, the distribution of cracks in the prestressed concrete with insufficient grouting material was more dispersed than those in the prestressed concrete with sufficient grouting material, and the spacing of the cracks was larger.

3.2 Strain Analysis

Based on the measured values from the concrete strain gauges in

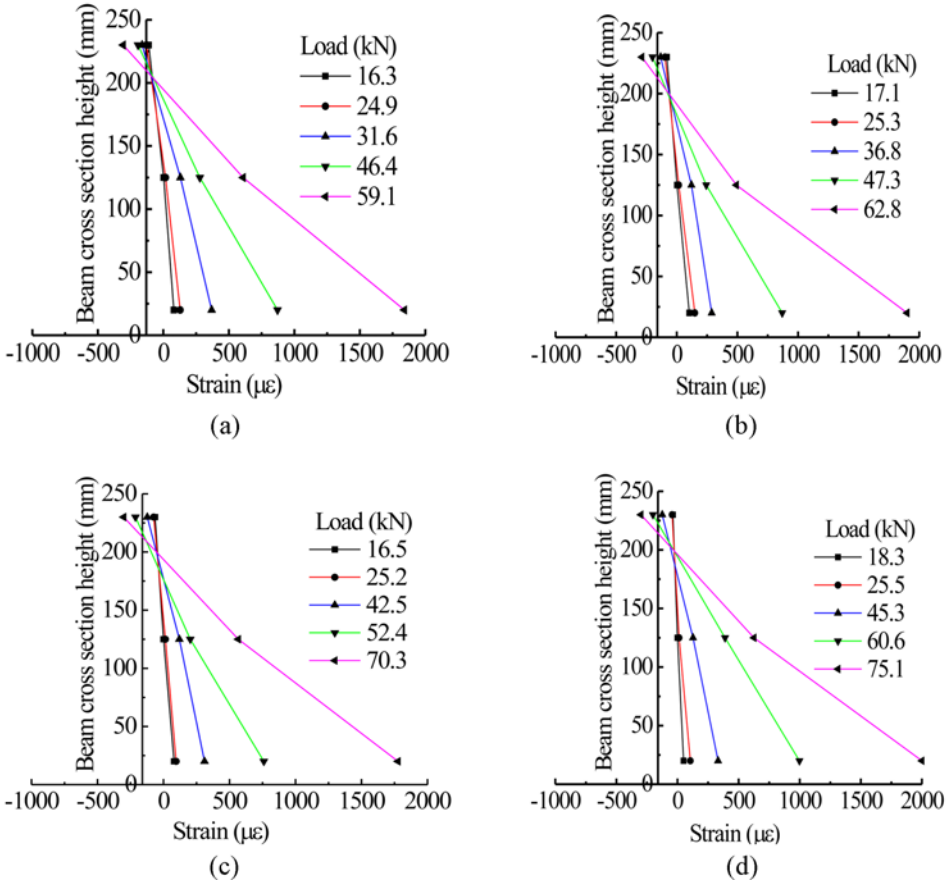

Fig. 6. Strain of the Concrete in the Midspan of the Metal Sheaths Prestressed Beam: (a) PCB1-1, (b) PCB1-2, (c) PCB1-3, (d) PCB1-4

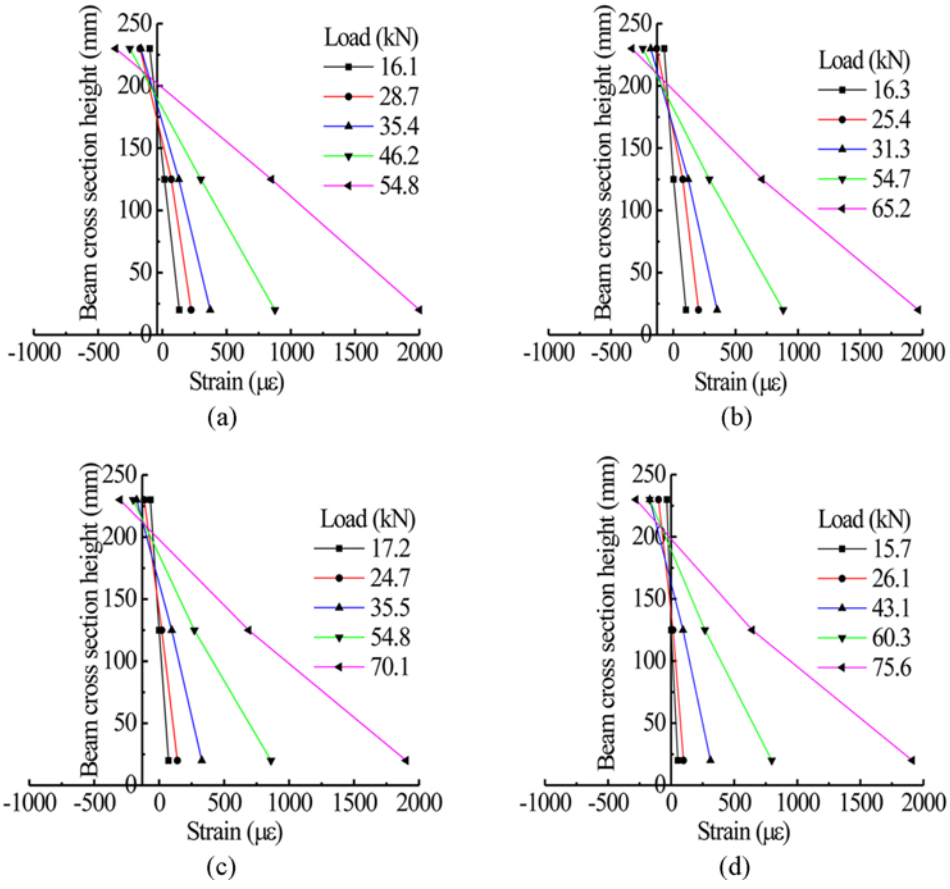

Fig. 7. Strain in the Concrete in the Midspan of the Plastic Sheaths Prestressed Beams: (a) PCB2-1, (b) PCB2-2, (c) PCB2-3, (d) PCB2-4

the prestressed concrete beams with tested prestressed concrete beams, several representative total loads were selected, and the concrete strain from the beginning of loading to the upper limit of the measuring range of the concrete strain gauges (or the bearing capacity of the test beams) were used to plot the midspan concrete strain curves along the beams, as shown in Figs. 6 and 7.

Figures 6 and 7 showed the midspan concrete strain distribution along the height of the prestressed concrete beams with different grouting compactnesses and corrugated tubes made of either metal or plastic materials under the external loads. During the loading process, the strain of the concrete in the compression and tension zones of the beams increased with increasing load. Under different load levels, the concrete strain in the midspan section of the beam varied linearly along the height of the beam.

The concrete strain curves of the midspan section of the two kinds of sheaths prestressed concrete beams showed that the concrete strain values and the height of the compression zone at the same positions of the beams were approximately equal before cracking under approximately similar loads, but after cracking, the concrete strain and the height of the compression zone were approximately equal for the beams with different grouting compactness of the holes when the forming materials of the holes were the same. Under similar load grades, the height of the compression zone of the beam increased with increasing grouting compactness of the channel. Therefore, when the other conditions were the same, the grouting compactness of the channel had less influence on the height of the compression zone of the section before cracking of the prestressed concrete beam but a more obvious influence on the height of the compression zone of the section after the cracking of the prestressed concrete beam. Increasing the grouting compactness of the channel can make full use of the strong compressive capacity of concrete and improve the flexural capacity of such beams.

3.3 Load-Deflection Curve

The deflection was determined using the equivalent moment of inertia method and compared with the measured deflection value in the test. Using the equivalent moment of inertia method the ratio between the calculated value and the measured value was determined. According to the measured deflection data of the test, considering the influence of different grouting fullness of the tunnel on the prestressed concrete beam, linear regression is performed on this ratio.

The load-displacement curves of the prestressed beams with different levels of grouting compactness of the metal and plastic sheaths can be obtained by displacement correction, as shown in Fig. 9. Coefficient of correction β was used to modify the deflection calculation formula of the equivalent moment of inertia method,

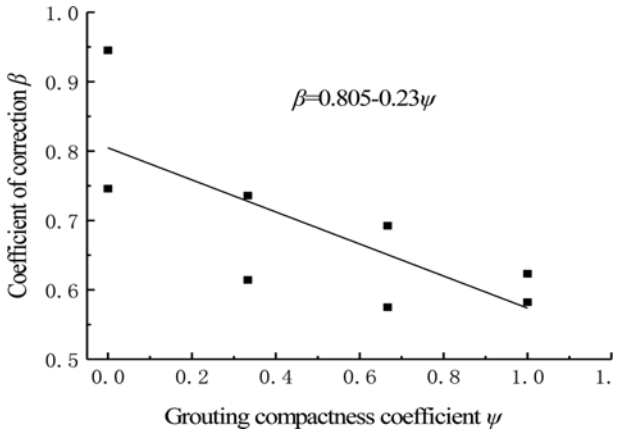

Fig. 8. Linear Regression Results

and the result of the linear regression was shown in Fig. 8.

The coefficient of correction β can be expressed as:

$$\beta = 0.805 - 0.23\psi \tag{1}$$

where ψ is the compactness coefficient.

The deflection f of the modified equivalent moment of inertia method can be expressed as:

$$f = \beta s \frac{M_s l^2}{B_s} \tag{2}$$

where s is the deflection coefficient in relation to the supporting condition and the load form; for the simply supported beam, s is chosen as $s = 0.1065$ due to the two point loads. M_s is the measured load, l is the calculated span of the beam, and B_s is the short-term flexural stiffness.

In Fig. 9, the effects of grouting compactness on the deflection of the prestressed beams were compared and analyzed. The load-deflection curve of each beam can be divided into three sections. Before cracking, the component deformation was very small. The midspan deflection of the prestressed beams with different levels of grouting compactness showed a linear trend with the increase of load, and the increase rate of deflection was slow. After cracking, as the load continued to increase, the midspan deflection of each test beam clearly increased at a faster rate than the rate before cracking. In addition, as the grouting density increased, the rate of increase of the deflection decreased. During the later stage of loading, even with a small increase in the load, the midspan deflection had a greater rate of increase until the components were crushed and did not continue to bear the load.

Figure 9 showed that the overall trends of the load-deflection curves of the prestressed beams with different grouting compactnesses were basically consistent, and the curves had only small differences in slope. Because the beam was in the elastic stage, the deformation was small, the midspan deflection difference was not apparent, and both types of beams had midspan deflections that linearly increased with the load. The curves clearly showed that the rate of increase in the deflection in the midspan of the test beams with different levels of grouting compactness varied in the course of loading, and all of the deflection curves showed a gradual increase with the load. Fig. 9 also showed that a denser grouting results in a greater slope of the curve and a lower rate of increase of the deflection. Under the same load level, despite the measurement error of individual data points, the deflection of prestressed beams with dense grouting was smaller than that of prestressed beams with uncompacted grouting. After cracking occurred in the concrete, the curves gradually decreased in slope, and the difference in the deflection in the beam was more apparent.

Figure 9 showed the bearing capacity of the prestressed beams with the same sheaths material increased with the grouting compactness. Regarding the test beams, the bearing capacity of the prestressed beam with dense grouting was more than 25% higher than that of the prestressed beam without grouting. The resistance and overall bearing capacity of the prestressed beams with metal sheaths were better than those of the prestressed beams with plastic sheaths with the same grouting compactness. The bearing capacity of the prestressed beams with metal sheaths can be increased by approximately 5% over that of the prestressed beams with plastic sheaths and the same grouting compactness. This result was mainly because the stress in the fully grouted concrete beam included the bond stress between the prestressed tendons and the surrounding concrete, and the tensile function of the prestressed tendons in the middle of the span can be fully utilized. For the prestressed beam with less dense grouting, due to the weakening of the bond stress between the prestressed tendons and the surrounding concrete, these two components can undergo relative longitudinal sliding. In addition, the stress values at each section were consistent, and the increase in the strain was equal to the average of the concrete strain along the full length of the prestressed beam. When the beam was in the state of bending and failure, the concrete at the section of the maximum bending moment reached the ultimate strain value, and the maximum strain of the prestressed tendons of the prestressed beam with less dense grouting was less than that of the beam with full grouting.

Before and after cracking, the formula for calculating midspan deflection of post-tensioned prestressed concrete beams was established by the equivalent inertia moment method, and it was revised considering the influence of grouting compactness. Compared with the measured midspan deflection, the modified Eq. (2) had higher accuracy. The comparison with the measured results was shown in Table 5.

By comparing the calculated results of the deflection correction formula using the equivalent moment of inertia method with the measured deflection results of the prestressed concrete beams, the average value of the ratio of the modified deflection to the measured deflection was 1.06, the standard deviation was 0.27, and the coefficient of variation was 0.25 (Table 5). The calculated results of the modified deflection calculation formula were in good agreement with the experimental results as a whole, indicating that the post-tensioned prestressed concrete beams were mixed properly. The modified formula of the equivalent moment of inertia method for calculating the midspan deflection of the concrete beams was reasonable and can provide some

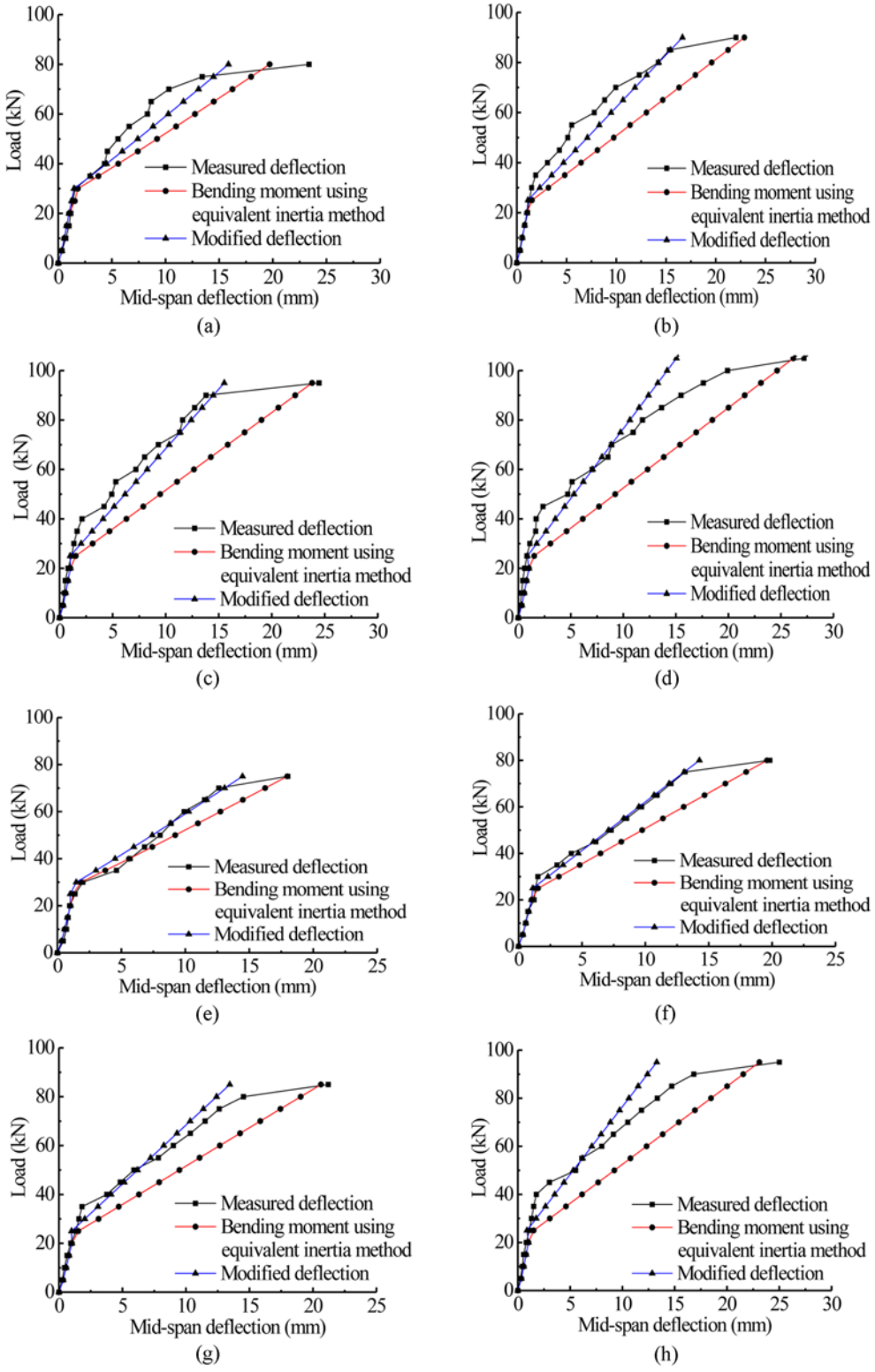

Fig. 9. Load-Deflection Curves of the Beams: (a) PCB1-1, (b) PCB1-2, (c) PCB1-3, (d) PCB1-4, (e) PCB2-1, (f) PCB2-2, (g) PCB2-3, (h) PCB2-4

reference for engineering calculations.

3.4 Ductility Analysis

In a low cyclic loading test, a skeleton curve can be obtained by connecting the peak point (unloading point) of every cycle of the load-displacement curve to form an enveloping line. The connection of all initial unloading points on the concrete constitutive curve was similar to the stress-strain curve of monotonic loading, so

Table 5. Contrastive Analysis of Measured Deflection and Corrected Value

Sample number	Grouting compactness	f^e_{cr}/mm	f^c_{cr}/mm	f^c_{cr}/f^e_{cr}	$\bar{y}=f^c/f^e$		
					Average value $\bar{y}$	Standard deviation σ	Coefficient variation δ
PCB1-1	0	1.61	1.25	0.78	1.05	0.21	0.20
PCB1-2	1/3	1.92	1.12	0.58	1.19	0.27	0.23
PCB1-3	2/3	2.15	0.99	0.46	1.23	0.30	0.24
PCB1-4	1	2.35	0.87	0.37	1.22	0.44	0.36
PCB2-1	0	1.41	1.25	0.89	0.83	0.14	0.17
PCB2-2	1/3	1.52	1.12	0.74	0.95	0.18	0.19
PCB2-3	2/3	1.84	0.99	0.54	0.99	0.24	0.24
PCB2-4	1	2.06	0.87	0.42	1.04	0.37	0.36

Table 6. Ductility Coefficients of Different Displacements

Sample number	Grouting compactness	Yield displacement (mm)	Ultimate displacement (mm)	Ductility coefficient (μ)
PCB1-1	Empty	8.89	20.38	2.32
PCB1-2	1/3	10.02	22.03	2.20
PCB1-3	2/3	11.34	24.46	2.16
PCB1-4	Dense	12.70	27.20	2.14
PCB2-1	Empty	7.46	18.01	2.41
PCB2-2	1/3	8.61	19.82	2.30
PCB2-3	2/3	9.63	21.21	2.21
PCB2-4	Dense	11.51	24.96	2.17

the monotonic loading-displacement curve equation can be regarded as the skeleton curve equation. The skeleton curve can also reflect the component yield displacement, cracking load and ultimate load. In this paper, the monotonic loading mode was chosen, and the load-displacement curve can be used instead of the skeleton curve to analyze the displacement ductility of the prestressed beams with different grouting compactnesses. In a broader sense, the ability of the structure to reflect the rotation of the plastic hinge section of a member, to absorb energy during dynamic loading, or to adapt to the settlement and volume deformation of the support was investigated. There were different definitions of the ductility of the components because of the research on different aspects of component ductility. Currently, some accepted and commonly used ductility indexes were as follows: the hysteretic curve, energy consumption ability, rotational ability of the plastic hinge, displacement ductility coefficient of the structure or component, and ductility coefficient of the section curvature. However, for the static analysis of components, the commonly used ductility indexes were the curvature ductility of the section and the displacement ductility coefficient. In this paper, the concept of the displacement ductility coefficient was used to define the ductility of prestressed beams with different levels of grouting compactness. The displacement ductility coefficient μ refers to the ratio of the ultimate displacement Δ_u to the yield displacement Δ_y of a member (Zhang et al., 2017), namely:

$$\mu = \frac{\Delta_u}{\Delta_y} \tag{3}$$

Table 6 showed the data of the destructive test of the prestressed simply supported beams with different levels of grouting compactness for metal sheaths and plastic sheaths. The displacement ductility coefficients of each member were obtained according to their load-displacement curves.

Table 6 showed that the ductility coefficient of the prestressed concrete beams decreased gradually with an increase in the grouting compactness when the same sheaths were used with different levels of grouting compactness. That is, the ductility of the prestressed concrete structure without full grouting was better than that with full grouting because the stress in the concrete beam with full grouting included the bond stress between the prestressed tendons and the surrounding concrete, and the stress of the prestressed tendon was greater in the middle section. Therefore, the cracks in the midspan of the beam were more concentrated. The cracks in the midspan developed with an increase in the load, and the prestressed tendons in the beam span yield more easily as the stress increased; the beam reached the limit state soon after yielding. For the prestressed beams without full grouting, the stress distribution of the prestressed tendons along the beam span was more uniform, there was no maximum stress point in the beam span, and the prestressed tendons did not easily yield.

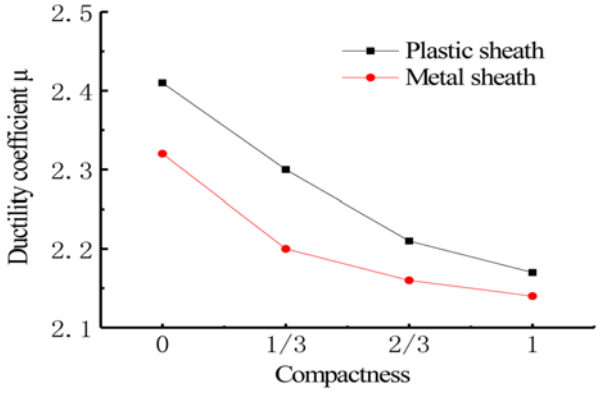

Fig. 10. Comparison of Ductility Coefficients

Figure 10 showed the contrasting curves of the ductility coefficients of the prestressed beams of metal and plastic sheaths with different levels of grouting compactness. The ductility of the prestressed beams with different sheaths material under different levels of grouting compactness was analyzed.

As seen from Fig. 10, the ductility coefficients of the metal and plastic corrugated prestressed concrete beams decreased with an increase in the grouting compactness. Therefore, the ductility of the prestressed concrete construction with insufficient grouting was better than that of the fully grouted prestressed concrete. That is, the unbonded prestressed beams were more ductile than the bonded prestressed beams. In addition, the ductility coefficient curve of the plastic sheaths was clearly and consistently above the ductility coefficient curve of the metal sheaths, but the curves became more similar with an increase in the grouting compactness. This finding meant that the ductility of the prestressed beams with plastic sheaths was better than that of the prestressed beams with metal sheaths. The difference in the ductility coefficient between the two kinds of sheaths was smaller when the grouting was denser. That is, the sheaths had little effect on the ductility of the beam when the grouting was dense.

3.5 Stiffness Analysis

To analyze the degradation law of short-term bending stiffness of test beams, the degradation law of the stiffness of the test beams was analyzed for different sections of the test beams, different channel grouting compactnesses and different channel-forming materials. To analyze the stiffness degradation law of different sections of prestressed concrete beams with different grouting compactnesses before and after cracking, taking PCB1-1, PCB1-2, PCB1-3 and PCB1-4 of the metal sheaths prestressed concrete beams as examples, the deflection curves of the 1/8, 1/4 and 1/2 sections of the loaded test beams were used to analyze the distribution of stiffness degradation along the length of the beams. Fig. 11 showed the load-deflection curves of the 1/8 section, 1/4 section and 1/2 section of each prestressed concrete beam.

Figure 11 showed that before the cracking of prestressed

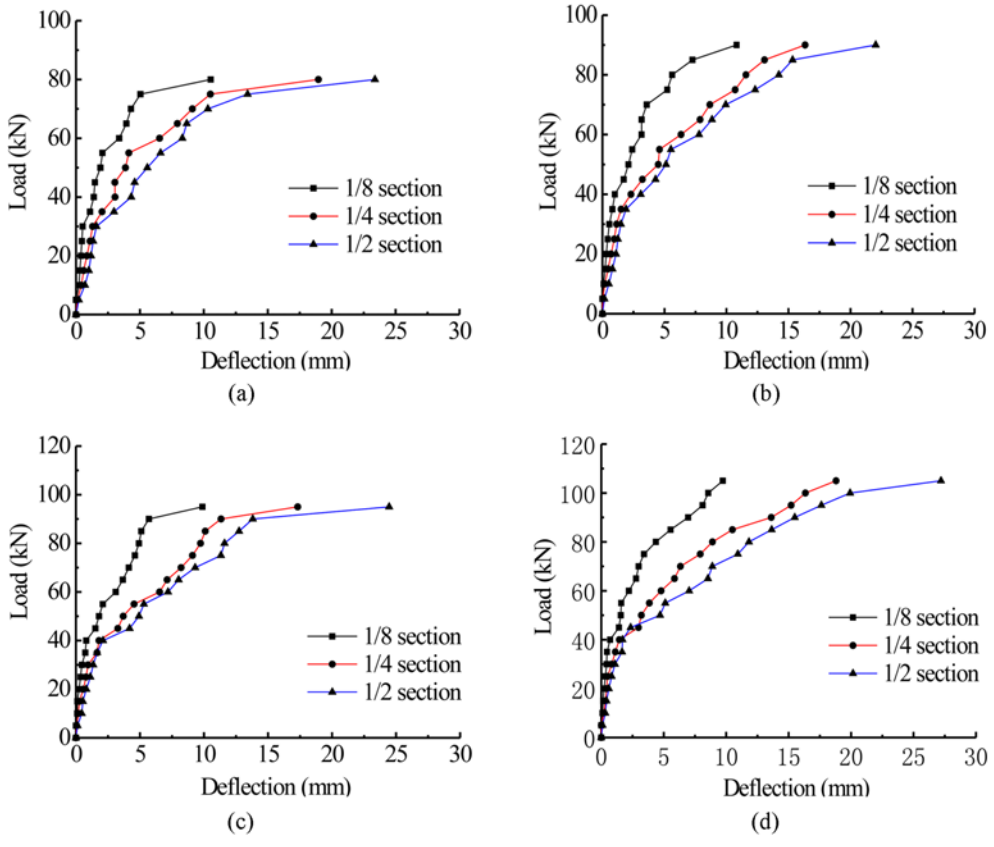

Fig. 11. Load-Deflection Curves of Various Sections: (a) PCB1-1, (b) PCB1-2, (c) PCB1-3, (d) PCB1-4

concrete beams with different grouting compactnesses, the beams were in the elastic stage. The load-deflection curves at the 1/8 section, 1/4 section and 1/2 section of the beams were basically linear, the deflection changes were small, and the stiffness along the midspan of the beams did not decrease. After concrete cracking, the deflection of each section increased rapidly. The deflection growth rate of the 1/2 cross-section was the largest, followed by that of the 1/4 cross-section, while that of the 1/8 cross-section was relatively slow. Therefore, the degradation rate of cross-section stiffness decreased gradually from the middle cross-section to both ends of the beam. That is, after concrete cracking, the stiffness degradation of prestressed concrete beams with different grouting compactnesses was severe. The degradation of stiffness of prestressed concrete beams mainly occurred in the stage from concrete cracking to steel yielding. To improve the bearing capacity of prestressed concrete beams, it was necessary to effectively control the degradation rate of the stiffness of the beams during this stage, especially in the middle of the span.

To analyze the effect of grouting compactness on the short-term stiffness of two kinds of prestressed beam sheaths, the influence curves of the prestressed beams with different levels of grouting compactness and with metal and plastic sheaths were drawn under the same load grade before and after cracking in Figs. 12 and 13, respectively.

Figures 12 and 13 showed that grouting compactness was one of the factors affecting the short-term stiffness of post-tensioned prestressed beams. A denser grouting resulted in a smaller deflection under the action of the same load, consequently resulting in a greater short-term stiffness of the beam. Before the beam cracks, the stiffness of a beam with full grouting was relatively low, and the deflection curve was relatively gentle. After the beam cracked, the curve steepened, and the rate of decrease in the midspan deflection increased with the grouting compactness. In addition, it can be seen from the prestressed beams with the same grouting porosity that under the same load, the midspan deflection of a prestressed beam with metal sheaths was smaller than that of a prestressed beam with plastic sheaths. Therefore, the stiffness of a prestressed beam with metal sheaths was better than that of a prestressed beam with plastic sheaths when the grouting porosity was the same.

According to the definition of stiffness, the slope of the load-deflection curve was proportional to the stiffness of the beam, and the stiffness of the prestressed concrete beam can be expressed by the load-deflection curve. The following was a comparative analysis of load-deflection curves of metal and plastic sheaths prestressed concrete beams under four conditions of grouting compactness: no grouting, 1/3 grout compactness, 2/3 grout compactness and complete grout compactness. The

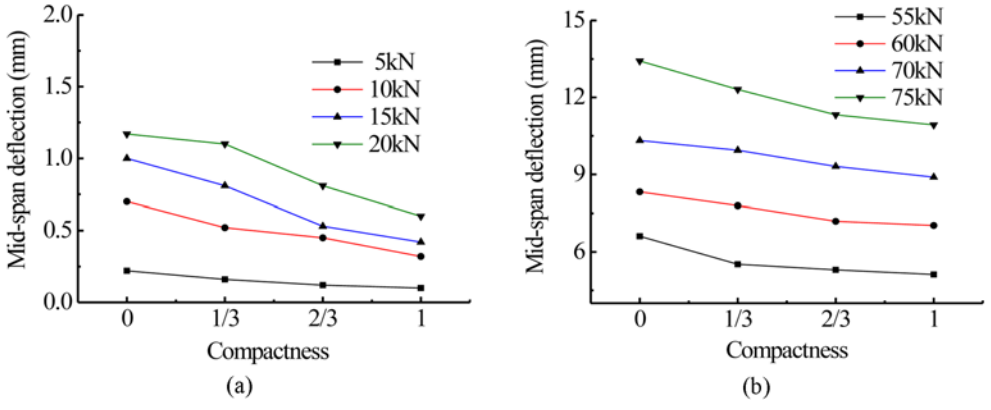

Fig. 12. Deflection Curve before and after Cracking of the Prestressed Beam with a Metal Sheath: (a) Before Cracking, (b) After Cracking

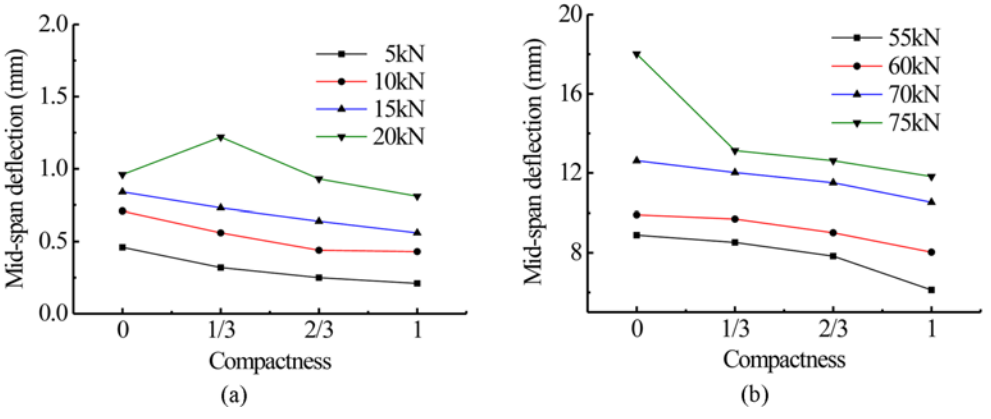

Fig. 13. Deflection Curve before and after Cracking of the Prestressed Beam with a Plastic Sheath: (a) Before Cracking, (b) After Cracking

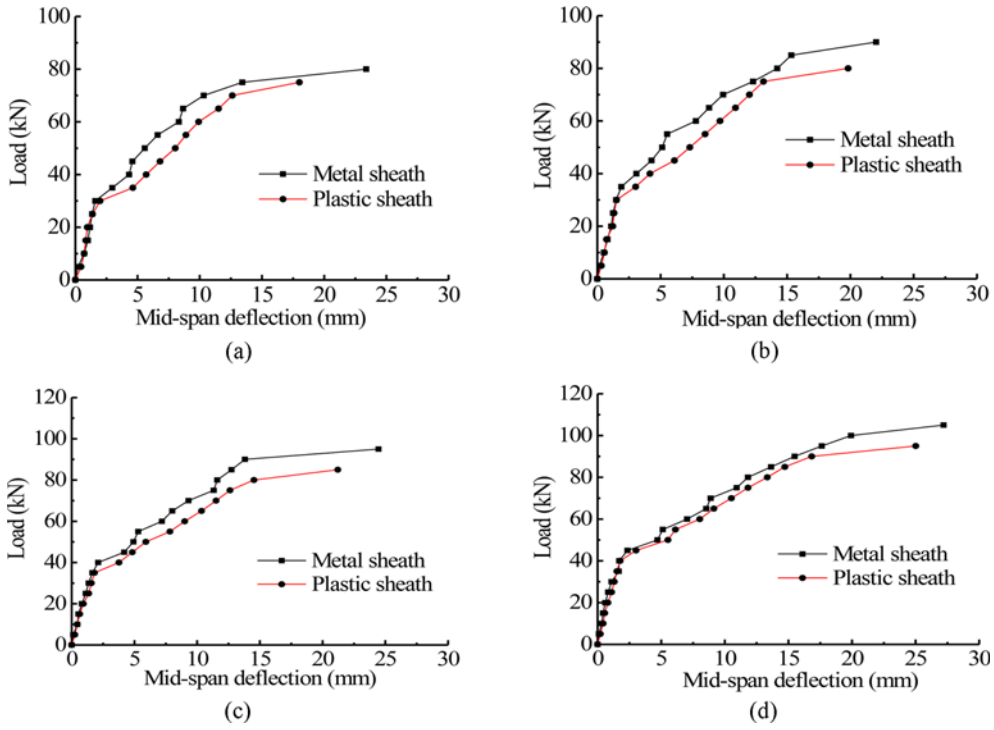

Fig. 14. Load-Deflection Curves: (a) No Grouting, (b) 1/3 Grout Compactness, (c) 2/3 Grout Compactness, (d) Complete Grout Compactness

influence of the grouting materials on the stiffness of prestressed concrete beams was analyzed, as shown in Fig. 14.

Figure 14 showed that the load-deflection curves of the precracked prestressed concrete beams with the same grouting compactness basically coincided, indicating that the stiffnesses of the prestressed concrete beams with sheaths fabricated from two different materials were basically the same. The slope of the load-deflection curve after cracking of the prestressed concrete beams with metal sheaths was greater than that of the prestressed concrete beams with plastic sheaths, meaning that the stiffness of the metal sheaths prestressed concrete beams was greater than that of the plastic sheaths prestressed concrete beams. Under certain grouting compactness conditions, the influence of grouting material on the stiffness of precracked prestressed concrete beams was small, but that on the stiffness of postcracked beams was significant.

4. Conclusions

In this paper, 4 prestressed concrete beams with metal sheaths and 4 prestressed concrete beams with plastic corrugated tubes with different degrees of grouting compactness were tested. Through execution of the test process, observation of the test phenomenon and analysis of the test data, the failure process, failure mode and strain law of prestressed concrete beams were analyzed in terms of the channel-forming material and channel grouting compactness. According to the experimental phenomenon observed during the test, the test data, sheath material, molding material, and grouting compactness of the channel were analyzed, and the main conclusions on the influence of the prestressed concrete beam deflection and stiffness degradation on the ductility were as follows:

1. With the increase of grouting compactness, the cracking load and ultimate load of the beam tended to increase; when the sheath materials were the same, the bearing capacity of the prestressed concrete beams with dense grouting was approximately 25% higher than that of the prestressed concrete beams without grouting; the bearing capacity of the metal sheaths prestressed concrete beams was higher than that of the plastic sheaths prestressed concrete beams, which was approximately 5%. Therefore, in engineering design, for a prestressed concrete structure with high bearing capacity, the metal sheaths bonded prestressed concrete structure was preferred, and the quality of the grouting should be strictly controlled to increase the compactness.
2. In the case of the same sheaths material, the displacement ductility coefficient of the prestressed concrete beam decreased with the increase of grouting compactness. The displacement ductility coefficient of prestressed concrete beams without grouting was approximately 14% – 19% higher than that of prestressed concrete beams with grouting compactness. In the case of the same grouting compactness, the ductility of the prestressed concrete beam with the plastic sheaths was better than the ductility of the prestressed concrete beam with the metal sheaths. The ductility of the prestressed concrete beams with plastic sheaths was better than that of the prestressed concrete beams with metal sheaths, and the increase in the displacement ductility coefficient was less

than 10%. The increase in the displacement ductility coefficient decreased with the increase in grouting compactness. The fuller the channel grouting is, the smaller the effect of the channel-forming material and the port grouting compactness on the displacement ductility coefficient of the prestressed concrete beam.

3. Based on the equivalent moment of inertia method about the prestressed concrete beam stiffness and deflection calculation, the coordinated unification of prestressed concrete beam stiffness and deflection calculation methods for different grouting compactnesses can better reflect the beam crack, flexural stiffness and deflection of the actual changes and have a certain reference value for engineering practice.

The influence degree of grouting compactness on prestressed concrete beams was different before and after cracking. Considering the influence of grouting compactness and grouting material, the laws of the midspan deflection, steel strain, crack development and stiffness degradation of the test beams was analyzed. The results showed that before the cracking of beams, grouting compactness and grouting material had different effects on midspan deflection and steel yielding of the beams. After cracking, with the increase in grouting compactness, the degradation rates of midspan deflection and the strain and stiffness of the longitudinal tensioned steel bars decreased, and the crack distribution became more concentrated as spacing decreases. When the grouting compactness was the same, the stiffness degradation of the metal sheaths prestressed concrete beams and the crack spacing were lesser than those of the plastic sheaths prestressed concrete beams. In summary, the stiffness degradation of prestressed concrete beams mainly occurred from cracking to steel yielding. If the stiffness degradation rate of prestressed concrete beams can be effectively controlled in this stage, their bearing capacity can be effectively improved.

Acknowledgements

This paper is a part of the National Natural Science Foundation of China (Grant number: 51968045), and a part of science and technology project in the Zhejiang Traffic Quality Supervision Bureau (Grant number: ZJ201602), and a part of science and technology project in China Railway 21st Bureau Group (Grant number: 14B-3), and a part of science and technology project in China Railway Construction Investment Group Co. Ltd. (Grant number: 16-C35).

ORCID

Not Applicable

References

Cao DF, Qin XC, Yuan SF (2013) Experimental study on mechanical behaviors of prestressed concrete beams subjected to freeze-thaw cycles. *China Civil Engineering Journal* 46(8):38-44, DOI: 10.15951/j.tmgcxb.2013.08.015 (in Chinese)

Deng JH, Shao XD (2013) Nonlinear analysis of prestressed concrete beam based on hybrid element method. *Engineering Mechanics* 30(10):171-177, DOI: 10.6052/j.issn.1000-4750.2012.07.0494

Dong SY (2010) Model test study on deflection of prestressed concrete simply supported beam after cracking. MSc Thesis, Chang' An University, Xi'an, China (in Chinese)

Du GC (1997) Application and development of prestressed concrete for buildings in china in the past 40 years. *China Civil Engineering Journal* 30(1):3-15, DOI: 10.15951/j.tmgcxb.1997.01.001 (in Chinese)

Du MM, Su XZ (2012) Research on crack width at different locations of post-tensioned bonded prestressed concrete beams with 500 MPa steel bars. *Journal of Building Structures* 33(9):141-147, DOI: 10.14006/j.jzjgxb.2012.09.008 (in Chinese)

Enrin H, Katsuki S, Ishikawa N, Ohta T (2000) The experimental study on dynamic flexural toughness of post-tension prestressed reinforced concrete beam under high speed loading. *Concrete Research & Technology* 11(1):19-27, DOI: 10.3151/crt1990.11.1_19

Farhidzadeh A, Salamone S (2015) Reference-free corrosion damage diagnosis in steel strands using guided ultrasonic waves. *Ultrasonics* 57:198-208, DOI: 10.1016/j.ultras.2014.11.011

Feng C, Yuan C, Guang ZQ, Lei G (2014) Experimental study of bellows duct grouting compactness with quantitative detection. *Applied Mechanics and Materials* 716-717:322-327, DOI: 10.4028/www.scientific.net/AMM.716-717.322

Jaime MF, Bischof P, Kaufmann W (2018) Exploiting the potential of digital fabrication for sustainable and economic concrete structures. 1st RILEM international conference on concrete and digital fabrication, September 10-12, Zurich, Switzerland

JGJ55-2011 (2010) Specification for mix proportion design of ordinary concrete. JGJ55-2011, China Architecture&Building Press, Beijing, China

Ji BH, Fu ZQ (2010) Analysis of Chinese bridge collapse accident causes in recent years. *China Civil Engineering Journal* 43(s1): 495-498, DOI: 10.15951/j.tmgcxb.2010.s1.010 (in Chinese)

Meng G, Jia JQ, Wang JZ (2013) Study on flexural behavior of prestressed ultra-high strength concrete beams. *Journal of Harbin Engineering University* 34(5):575-580, DOI: 10.3969/j.issn.1006-7043.201210060 (in Chinese)

Minh H, Mutsuyoshi H, Niitani K (2007) Influence of grouting condition on crack and load-carrying capacity of post-tensioned concrete beam due to chloride-induced corrosion. *Construction & Building Materials* 21(7):1568-1575, DOI: 10.1016/j.conbuildmat.2005.10.004

Minh H, Mutsuyoshi H, Taniguchi H, Niitani K (2008) Chloride-induced corrosion in insufficiently grouted post-tensioned concrete beams. *Journal of Materials in Civil Engineering* 20(1):85-91, DOI: 10.1061/(ASCE)0899-1561(2008)20:1(85)

Moini M, Jan O, Youngblood JP, Magee B, Zavattieri PD (2018) Additive manufacturing and performance of architectured cement-based materials. *Advanced Materials* 30(43):1-11, DOI: 10.1002/adma.201802123

Park H, Jeong S, Lee SC, Chou JY (2016) Flexural behavior of post-tensioned prestressed concrete girders with high-strength strands. *Engineering Structures* 112:90-99, DOI: 10.1016/j.engstruct.2016.01.004

Rupf M, Ruiz MF, Muttoni A (2013) Post-tensioned girders with low amounts of shear reinforcement: Shear strength and influence of flanges. *Engineering Structures* 56(6):357-371, DOI: 10.1016/j.engstruct.2013.05.024

Wang TW (2013) Civil engineering structural test - Part 1, 3rd edition. Wuhan University of Technology Press, Wuhan, China, 9-11

Wang L, Zhang X, Zhang J, Ma YF, Xiang YB, Liu YM (2014) Effect of insufficient grouting and strand corrosion on flexural behavior of PC beams. *Construction and Building Materials* 53:213-224, DOI: 10.1016/j.conbuildmat.2013.11.069

Woodward RJ (1990) Collapse of a segmental post-tensioned concrete bridge. Transportation Research Board, Washington, DC, USA, 38-59

Wu JY, Liu XJ (2013) Present situation and development of compactness detection technology of prestressed duct grouting. *Municipal Technology* 31(4):17-22

Zhang PF (2007) Investigation of grouting in the channel of bridge and performance analysis of tendon and its influence on bridge structure. MSc Thesis, Southeast University, Nanjing, China (in Chinese)

Zhang YT, Zhang J, Yang L (2017) Research on the effects of prestressing ratio on the seismic capacity of prestressed concrete frame structures. *Engineering Mechanics* 34(2):129-136, DOI: 10.6052/j.issn.1000-4750.2015.07.0580

Zhou JM, Pan XH, Zhang F (2013) Experimental study on seismic performance of post-tensioned prestressed concrete beams reinforced with 500 MPa rebars. *China Civil Engineering Journal* 46(5):39-49, DOI: 10.15951/j.tmgcxb.2013.05.015 (in Chinese)

Zhou SL, Zhang F, CaoY (2014) The experimental study of ultrasonic testing prestressed bellows pore grouting quality. *Applied Mechanics and Materials* 711:461-468, DOI: 10.6052/j.issn.1000-4750.2015.07.0580

Zhu EY (2012) Prestressed structure of modern bridge - Part 1, 4th and 5th edition. Tsinghua University Press and Beijing Jiaotong University Press, Beijing, China,14-18